ChemComm

Synthesis of Porous Coordination Polymers using Carbon Dioxide as a Direct Source

Journal:	*ChemComm*
Manuscript ID	CC-COM-06-2019-004771.R2
Article Type:	Communication

COMMUNICATION

Synthesis of Porous Coordination Polymers using Carbon Dioxide as a Direct Source

Received 00th January 20xx,
Accepted 00th January 20xx

DOI: 10.1039/x0xx00000x

Kentaro Kadota,[a] Nghia Tuan Duong,[b] Yusuke Nishiyama,[b,c] Easan Sivaniah,[a,d] and Satoshi Horike*[d,e,f,g]

Porous coordination polymers (PCPs) were synthesized by use of CO_2 and metal borohydrides as precursors. Borohydrides converted CO_2 into bridging ligands such as formate (HCO_2^-) or formylhydroborate ($[BH(OCHO)_3]^-$) which are available to construct porous architectures, one of them shows 380 $m^2 g^{-1}$ of surface area.

Carbon dioxide (CO_2) is an attractive renewable C1 building block with advantages such as abundance, availability and nontoxicity.[1-3] Synthetic routes and catalysts to convert CO_2 into fuels,[4-6] valuable chemicals[7-9] and functional materials have been explored.[10] Due to inherent inertness of CO_2, reactive reagents are a key for the activation of CO_2 in the material syntheses. For instance, organic polymers are produced from CO_2 with reactive monomers such as epoxides and dienes, and the products achieve a certain contents of CO_2 (10 – 40 wt%) in the structures.[11, 12] On the other hand, it is a challenge to explore the new synthetic protocols not only for organic polymers but other functional materials using CO_2 as a building block.

Porous coordination polymers (PCPs) or metal–organic frameworks (MOFs) are emerging materials designed by coordination bonds of metal ions and bridging ligands for functions of gas storage/separation, heterogeneous catalysis, magnetism, and electronic/ionic conductivity.[13-15] In spite of their large attention as materials, there is little report on the synthesis of PCPs by use of CO_2. This is because of a challenge to convert CO_2 into ligands in parallel with formation of a porous structure. In this work, we demonstrate the synthesis of PCPs from CO_2 using metal borohydrides with tunable reactivity, and investigate the porous properties.

Borohydride (BH_4^-) is a hydride-based complex anion and commonly used as reducing agents. Electron-donating BH_4^- reacts with CO_2 at mild conditions. The first reaction of BH_4^- and CO_2 was reported in 1950; $LiBH_4$ reacts with CO_2 in diethyl ether to produce lithium formate and diborane.[16] The reaction pathways of BH_4^- and CO_2 are classified as follows (Figure 1); hydride transfer from BH_4^- to CO_2 to form formate (HCO_2^-) and CO_2 insertion into B–H bond to form formylhydroborate ($[BH(OCHO)_3]^-$). The HCO_2^- and $[BH(OCHO)_3]^-$ could be used as bridging ligands to construct PCPs. Porous $[M_3(HCO_2)_6]$ have been constructed from various divalent metal ions and studied for N_2/CH_4 separation (Mn^{2+}),[17] magnetic properties (Fe^{2+}, Co^{2+})[18] and as a model of gas diffusion (Mg^{2+}).[19] They are synthesized from formic acid (HCO_2H) or the hydrolysis of *N*,*N*-dimethylformamide (DMF).

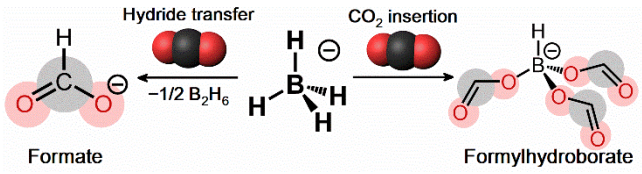

Figure 1. Reaction pathways of BH_4^- and CO_2.

We utilized both pure CO_2 and 400 ppm of CO_2 in compressed air under mild conditions for the synthesis of $[M_3(HCO_2)_6]$. The counter metal ions affect the reactivity of BH_4^- toward CO_2. Electronegative metal ions (Zn^{2+}, Ni^{2+}, Ru^{2+}) lead to the formation of HCO_2^- rather than $[BH(OCHO)_3]^-$.[20] Based on the trend, we applied $[PPh_4][Zn(BH_4)_3]$ as a precursor to produce HCO_2^- (Figure 2A). An acetonitrile (MeCN) solution of $[PPh_4][Zn(BH_4)_3]$ (50 mM) was reacted with atmospheric pressure of CO_2 (> 99.995%) at a flow rate of 60 mL min^{-1} at

[a] *Department of Molecular Engineering, Graduate School of Engineering, Kyoto University, Katsura, Nishikyo-ku, Kyoto 615-8510, Japan*
[b] *NMR Science and Development Division, RIKEN SPring-8 Center and RIKEN-JEOL Collaboration Center, Yokohama, Kanagawa 230-0045, Japan*
[c] *JEOL RESONANCE Inc., Musashino, Akishima, Tokyo 196-8558, Japan*
[d] *Institute for Integrated Cell-Material Sciences, Institute for Advanced Study, Kyoto University, Yoshida, Sakyo-ku, Kyoto 606-8501, Japan*
[e] *AIST-Kyoto University Chemical Energy Materials Open Innovation Laboratory (ChEM-OIL), National Institute of Advanced Industrial Science and Technology (AIST), Yoshida-Honmachi, Sakyo-ku, Kyoto 606-8501, Japan*
[f] *Department of Synthetic Chemistry and Biological Chemistry, Graduate School of Engineering, Kyoto University, Katsura, Nishikyo-ku, Kyoto 615-8510, Japan*
[g] *Department of Materials Science and Engineering, School of Molecular Science and Engineering, Vidyasirimedhi Institute of Science and Technology, Rayong 21210, Thailand*
Electronic Supplementary Information (ESI) available: [details of any supplementary information available should be included here]. See DOI: 10.1039/x0xx00000x

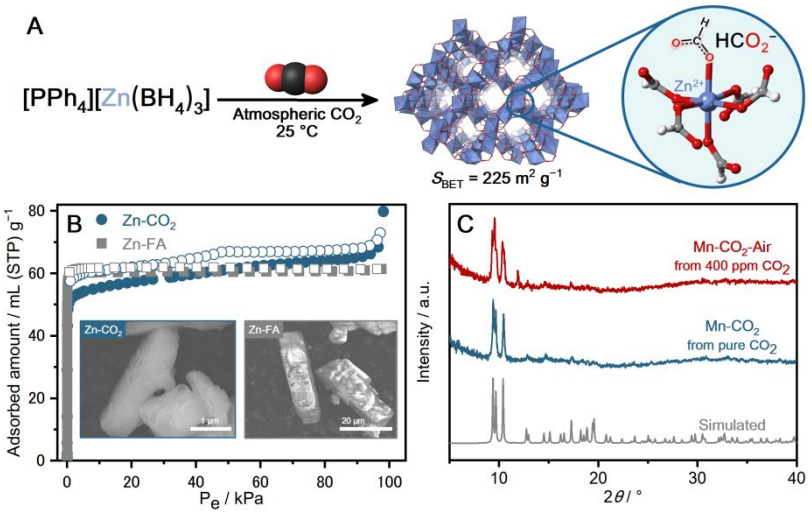

Figure 2. (A) Synthetic scheme of **Zn-CO₂** using atmospheric pressure of CO_2. (B) N_2 adsorption isotherms at 77 K for **Zn-CO₂** (blue) and **Zn-FA** (gray). The inset displays SEM images of **Zn-CO₂** (left) and **Zn-FA** (right). (C) PXRD patterns of simulated $[Mn_3(HCO_2)_6]$ (gray), **Mn-CO₂** (blue) and **Mn-CO₂-Air** (red).

25 °C. Aprotic MeCN is chosen because CO_2 shows good solubility in MeCN (270 mM at 25 °C)[21] and MeCN accelerates the rate of the hydride reduction of CO_2 to HCO_2^-.[22] White precipitate was formed in 40 min and isolated by filtration, which is denoted as **Zn-CO₂**. Powder X-ray diffraction (PXRD) pattern of **Zn-CO₂** matches with the simulated pattern of $[Zn_3(HCO_2)_6]$ (Figure S1). NMR spectra (^1H, ^{11}B, ^{13}C) of the **Zn-CO₂** digested in DMSO-d_6 indicate the formation of HCO_2^- without impurity (Figure S2–4, 58.4% yield). Note that CO_2 reduction and the crystallization of PCP occur in one-pot at 25 °C. For comparison, the same $[Zn_3(HCO_2)_6]$ was synthesized from HCO_2H via the reported method (denote as **Zn-FA**).[23] **Zn-CO₂** exhibits a slightly lower thermal stability than **Zn-FA** according to the TGA under Ar (240 vs. 270 °C, Figure S6). N_2 adsorption isotherms of the samples at 77 K are slightly different as shown in Figure 2B. The uptake amounts at a low pressure (1.02 kPa) for **Zn-CO₂** is lower than that of **Zn-FA**, but the total uptake amount at 96.6 kPa for **Zn-CO₂** is higher than **Zn-FA**. Brunauer–Emmett–Teller surface areas (S_{BET}) of **Zn-CO₂** and **Zn-FA** are 224.6 and 243.1 $m^2\ g^{-1}$, respectively. The uptake amount of CO_2 for **Zn-CO₂** at 195 K is higher than that of **Zn-FA** (98.5 vs. 73.2 mL g^{-1}, Figure S7). Scanning electron microscopy (SEM) was performed to study the morphological difference in **Zn-CO₂** and **Zn-FA** (Figure 2B). Although both are characteristic of rod-shaped crystallite, the particle size of **Zn-CO₂** is smaller than that of **Zn-FA** (Figure S9, **Zn-CO₂**: 4 – 20 μm, **Zn-FA**: 15 – 70 μm). High reactivity of BH_4^- toward CO_2 leads to fast reaction kinetics, resulting in a rapid crystal growth. **Zn-CO₂** has a layered structure in the rod-shaped crystallite, whereas **Zn-FA** has a relatively smooth surface. The layered structure of **Zn-CO₂** crystallite causes the mesoporous property observed in the N_2 adsorption isotherm.[24]

To apply this synthetic method to the other metal ions, we used alkylammonium borohydride salt, $[NR_4][BH_4]$, as BH_4^- source. $[NEt_4][BH_4]$ reacts with CO_2 to produce $[NEt_4][BH(OCHO_3)]$ and the accompanying hydrolysis of $[BH(OCHO_3)]^-$ produces HCO_2^-.[20] The reaction of $[NEt_4][BH_4]$ and 2.0 MPa of CO_2 at 25 °C provided $[NEt_4][BH(OCHO_3)]$ in a quantitative yield, which was confirmed by ^{11}B NMR and electrospray ionization mass spectroscopy (ESI-MS, Figure S10–11). Without isolation, a MeCN solution of $[NEt_4][BH(OCHO_3)]$ was mixed with a MeOH solution of MCl_2 (M = Mg^{2+}, Mn^{2+}, Fe^{2+}, Co^{2+}). The mixtures were heated at 70 °C, and crystalline $[M_3(OCHO)_6]$ (M = Mg^{2+}, Mn^{2+}, Fe^{2+}, Co^{2+}) were all isolated (denoted as **M-CO₂**, Figure 2C and S12). Structures of four **M-CO₂** were confirmed by PXRD and they exhibit gas adsorption properties comparable to the previous reports, as summarized in Figure S17. We tried to use 400 ppm of CO_2 in the air. The air gas was bubbled into a MeCN solution of $[NEt_4][BH_4]$ at a flow rate of 60 mL min^{-1} at 25 °C for 30 hours. The obtained solution was mixed with a MeOH solution of $MnCl_2$, and the solvothermal reaction provided crystalline $[Mn_3(HCO_2)_6]$ (**Mn-CO₂-Air**) in 11.6% yield as shown in Figure 2C. A low concentration of CO_2 is also available with BH_4^- and metal salts to construct the porous frameworks.

We next attempted to employ $[BH(OCHO)_3]^-$ as a bridging ligand (Figure 1). Two coordination polymers containing $[BH(OCHO)_3]^-$ were reported ([Na(1,2-dimethoxyehane)][$BH(OCHO)_3$] and K[$BH(OCHO)_3$]).[20, 25] Both of them are dense, nonporous structures due to the high coordination numbers (Na^+: 6, K^+: 9). Based on the trend of reactivity, we chose electropositive Mg^{2+} to form $[BH(OCHO)_3]^-$ from CO_2, and the corresponding borohydride salt, $Mg(BH_4)_2$ is highly soluble in organic solvents. We tested reactions using high pressure CO_2 with $Mg(BH_4)_2$ to promote CO_2 insertion pathway, and the optimized condition to obtain a porous structure (Figure 3). An MeCN solution of $Mg(BH_4)_2$ (50 mM) was reacted with CO_2 (> 99.995%) in a glass-lined high pressure vessel at 25 °C for 2 hours by varying the CO_2 pressure (2.0, 3.0, 4.0 MPa). Each reaction provided white suspension and colorless monolith was obtained after filtration in Figure 3A. Powder samples were obtained by drying at 25 °C under vacuum, denoted as **Mg-XMPa**, X = 2, 3, 4, respectively. PXRD of the samples were collected after drying at 25 °C under

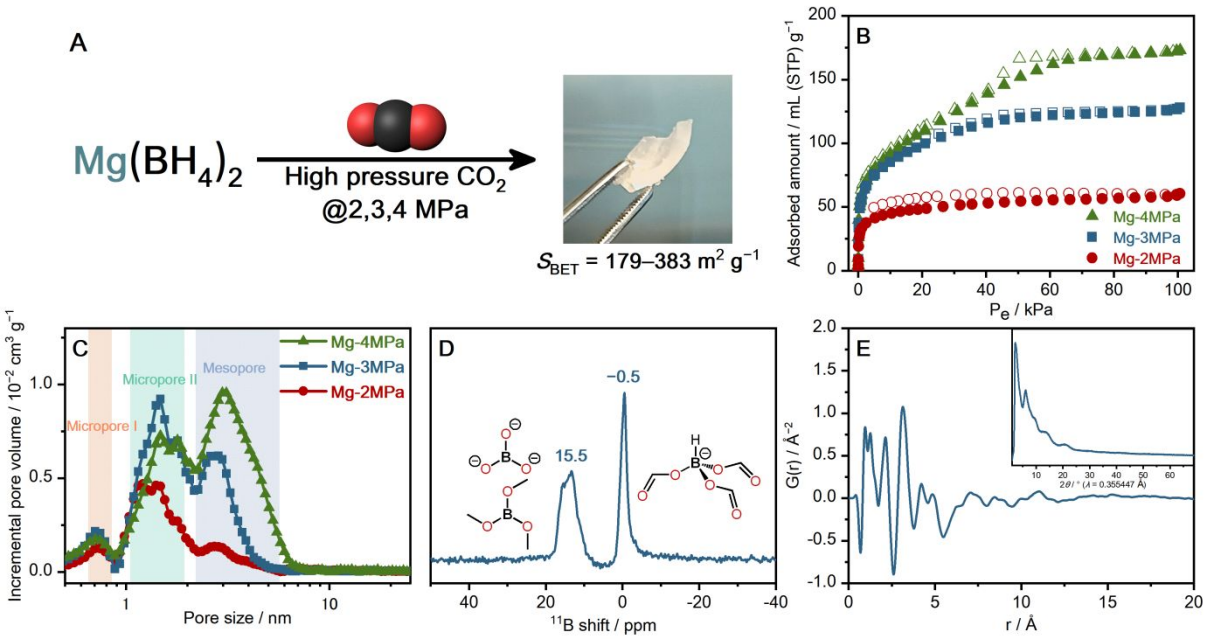

Figure 3. (A) Schematic illustration of formation of **Mg-XMPa**. The image displays monolith particle of **Mg-3MPa**. (B) N_2 isotherms at 77 K for **Mg-2MPa** (red circle), **Mg-3MPa** (blue square) and **Mg-4MPa** (green triangle). (C) Pore size distributions calculated using the NLDFT method for **Mg-XMPa**. (D) Solid-state ^{11}B MAS NMR spectrum of **Mg-3MPa**. (E) Reduced PDF of **Mg-3MPa**. Inset: total X-ray scattering of **Mg-3MPa**.

vacuum. No Bragg reflection was observed, indicating the products are amorphous, because of ligand flexibility (Figure S22). The samples exhibit similar infrared (IR) spectra characteristic of C=O stretching peak at 1600 cm^{-1}, which indicates the incorporation of CO_2 (Figure S23). Thermal properties were studied by TGA under Ar flow, and no weight loss was observed below 100 °C (Figure S24).

All the samples show permanent porosity from N_2 adsorption isotherms at 77 K (Figure 3B), and higher pressure of CO_2 in the synthesis enhances the total uptake amounts and S_{BET} (60.6, 128.1, 172.9 mL g^{-1} and 179.3, 356.4, 382.6 m^2 mg^{-1} for **Mg-2, 3, 4MPa**, respectively). **Mg-2MPa** exhibits a Type-I isotherm characteristic of a steep in N_2 uptake in a lower pressure region. In contrast, a gradual N_2 uptake for **Mg-4MPa** at a higher pressure region is observed in mesoporous structures. Pore size distributions were calculated from the N_2 adsorption isotherms using the non-local density functional theory (NLDFT) method (Figure 3C). **Mg-XMPa** are hierarchical porous structures, which include two types of micropores (micropore I: 0.7 nm, micropore II: 1.5 nm) and one mesopore at 2.7 nm. Non-crystalline porous materials such as porous organic polymers[26, 27] and glassy PCPs[28] are of interest as well as crystalline materials.

Solution and solid-state NMR measurements were carried out to determine chemical composition of **Mg-3MPa**. **Mg-3MPa** slightly dissolves in DMSO, and ^{11}B NMR spectrum of **Mg-3MPa** in DMSO-d_6 displays the peak of $[BH(OCHO)_3]^-$ (Figure S29). ^{1}H and ^{13}C NMR spectra of the **Mg-3MPa** digested in D_2O indicate that **Mg-3MPa** contains $–HCO_2$ and –OMe, $CH_3CH_2NH^-$ in a ratio of 36: 3: 2 from ^{1}H intensities (Figure S30, 32). $CH_3CH_2NH_2^-$ is originated from a reduction of MeCN.[29] ^{11}B NMR spectrum shows a broad peak of boric acid, $B(OH)_3$, formed by hydrolysis of $[BH(OCHO)_3]^-$ (Figure S31, Scheme S1). Solid-state ^{11}B NMR spectrum exhibits two peaks at −0.5 and 15.5 ppm corresponding to $[BH(OCHO)_3]^-$ and B–3O species such as $B(OMe)_3$ and BO_3^{3-}, respectively (Figure 3E).[20, 25] These assignments were confirmed by ^{1}H-{^{13}C} double cross polarization NMR experiment (Figure S44). The formation of $B(OMe)_3$ was reported by the reaction of KBH_4 and CO_2.[25] Furthermore, ^{11}B-^{11}B correlation NMR spectrum exhibits a distinct correlation between the boron nuclei of $[BH(OCHO)_3]^-$ and B–3O species, which indicates a homogenous distribution of each species in atomic scale (Figure S46). Consequently, a formula of **Mg-3MPa** was determined as $[Mg_{13}[BH(OCHO)_3]_{12}(BO_3)_4[B(OMe)_3](CH_3CH_2NH)_2]$ based on the results of NMR and elemental analysis (EA). According to this, the CO_2 content in the structure is 68.5 wt%. **Mg-2, 4MPa** have a similar composition with **Mg-3MPa** based on EA (Table S1).

The coordination environments around Mg^{2+} were studied by X-ray absorption spectroscopy (XAS) collected using synchrotron soft X-ray under high vacuum (Figure S47). The spectrum with low S/N ratio in the extended X-ray absorption fine structure (EXAFS) region was obtained, which is commonly observed for light element Mg. Meanwhile, the X-ray absorption near edge structure (XANES) spectrum of **Mg-3MPa** is similar to that of $[Mg_3(OCHO)_6]$ having Mg–6O. This implies that **Mg-3MPa** contains Mg–6O, which agrees with the fact that Mg^{2+} complexes prefer Mg–6O geometry (Figure S28). To further characterize the structure in longer length scale, synchrotron X-ray scattering measurement was performed on **Mg-3MPa** in Figure 3E. The corresponding reduced pair distribution function (PDF), which is atom–atom distance histograms, of **Mg-3MPa** was extracted after appropriate data corrections. The correlations below 5 Å assigned to B–O/ C–O

(1.2 Å), Mg–O (2.1 Å), Mg–C (3.1 Å) and Mg–B (4.9 Å) in reference to the reported $[BH(OCHO)_3]^-$ structures (Figure S48–49). In longer range order, three peaks are observed up to 11.1 Å, including Mg^{2+}–Mg^{2+} correlation. The periodicity in the longer range implies the formation of extended coordination network in **Mg-3MPa**.

With these results, we illustrated the proposed porous networks of **Mg-3MPa** (Figure S50). It is successful to construct porous structures using $[BH(OCHO)_3]^-$ and B–3O species. Key synthetic parameters are; (i) MeCN is essential to form porous network. The control experiment (THF, DMSO) provided no solid product or non-porous product (Et_2O, Figure S27). (ii) The tritopic bridging ligand $[BH(OCHO)_3]^-$, BO_3^{3-} and $B(OMe)_3$ would play a role in preventing the formation of a dense structure.[30] Although **Mg-2, 3, 4MPa** have no significant difference in the chemical compositions from ^1H NMR and EA, distinct porous structures are observed (Figure S35–37, Table S1, 2). In particular, mesopores are more generated as the CO_2 pressure increases in the synthesis (Figure S26). The result indicates that higher CO_2 pressure kinetically induces the formation of porous structure.[31] The tunable hierarchical porous structures are potentially applicable to small molecule separation/transport.

In conclusion, we demonstrated the synthesis of PCPs by use of the reactions of CO_2 and metal borohydride salts. Formation of HCO_2^- and $[BH(OCHO)_3]^-$ both of which work as bridging ligands was regulated by the electronegativity of metal ions. Crystalline $[M_3(HCO_2)_6]$ (**M-CO_2, Mn-CO_2-Air**) were synthesized from pure or 400 ppm of CO_2. The reaction of high pressure of CO_2 and $Mg(BH_4)_2$ preferred to form another ligand $[BH(OCHO)_3]^-$, resulting amorphous PCP $[Mg_{13}[BH(OCHO)_3]_{12}[BO_3]_4[B(OMe)_3][CH_3CH_2NH]_2)]$ (**Mg-XMPa**) with hierarchical porosity. CO_2 pressure in syntheses affects the ratio of micropore and mesopore, and high porosity (S_{BET} = 380 $m^2\ g^{-1}$) was observed. The approach provides a new perspective on the utilization of CO_2 toward the synthesis of functional materials – PCP/MOFs under mild conditions.

The work was supported by the Japan Society of the Promotion of Science (JSPS) for a Grant-in-Aid for Scientific Research (B) (JP18H02032) from the Ministry of Education, Culture, Sports, Science and Technology, Japan, and Strategic International Collaborative Research Program (SICORP) and Adaptable and Seamless Technology Transfer Program through Target-driven R&D (A-STEP) from the Japan Science and Technology, Japan. X-ray total scattering measurement was carried out at the BL02B2 of Super Photo Ring, Hyogo, Japan. Mg XAS experiments were conducted at the BL1N2 of Aichi Synchrotron Radiation Center, Aichi Science & Technology Foundation, Aichi, Japan (Proposal No. 201706136). K.K. thanks Mr. Yutaka Hirooka at Imamura Sanso Co., Ltd. for the helpful advice on CO_2 experimental system design.

Conflicts of interest

The authors declare no conflict of interest.

Notes and references

1. T. Sakakura, J.-C. Choi and H. Yasuda, *Chem. Rev.*, 2007, **107**, 2365-2387.
2. Q. Liu, L. Wu, R. Jackstell and M. Beller, *Nat. Commun.*, 2015, **6**, 5933.
3. J. Artz, T. E. Muller, K. Thenert, J. Kleinekorte, R. Meys, A. Sternberg, A. Bardow and W. Leitner, *Chem. Rev.*, 2018, **118**, 434-504.
4. G. A. Olah, A. Goeppert and G. K. S. Prakash, *J. Org. Chem.*, 2009, **74**, 487-498.
5. J. Wei, Q. Ge, R. Yao, Z. Wen, C. Fang, L. Guo, H. Xu and J. Sun, *Nat. Commun.*, 2017, **8**, 15174.
6. S. Kato, S. K. Matam, P. Kerger, L. Bernard, C. Battaglia, D. Vogel, M. Rohwerder and A. Zuttel, *Angew. Chem. Int. Ed.*, 2016, **55**, 6028-6032.
7. A. S. Lindsey and H. Jeskey, *Chem. Rev.*, 1957, **57**, 583-620.
8. R. Martin and A. W. Kleij, *ChemSusChem*, 2011, **4**, 1259-1263.
9. K. Huang, C. L. Sun and Z. J. Shi, *Chem. Soc. Rev.*, 2011, **40**, 2435-2452.
10. M. Aresta, A. Dibenedetto and A. Angelini, *Chem. Rev.*, 2014, **114**, 1709-1742.
11. R. Nakano, S. Ito and K. Nozaki, *Nat. Chem.*, 2014, **6**, 325-331.
12. S. Inoue, H. Koinuma and T. Tsuruta, *Makromol. Chem.*, 1969, **130**, 210-220.
13. O. M. Yaghi, M. O'Keeffe, N. W. Ockwig, H. K. Chae, M. Eddaoudi and J. Kim, *Nature*, 2003, **423**, 705-714.
14. S. Kitagawa, R. Kitaura and S. Noro, *Angew. Chem. Int. Ed.*, 2004, **43**, 2334-2375.
15. G. Férey, *Chem. Soc. Rev.*, 2008, **37**, 191-214.
16. J. G. Burr, W. G. Brown and H. E. Heller, *J. Am. Chem. Soc.*, 1950, **72**, 2560-2562.
17. D. N. Dybtsev, H. Chun, S. H. Yoon, D. Kim and K. Kim, *J. Am. Chem. Soc.*, 2004, **126**, 32-33.
18. Z. Wang, B. Zhang, Y. Zhang, M. Kurmoo, T. Liu, S. Gao and H. Kobayashi, *Polyhedron*, 2007, **26**, 2207-2215.
19. M. Fischer, *Micropor. Mesopor. Mater.*, 2016, **219**, 249-257.
20. I. Knopf and C. C. Cummins, *Organometallics*, 2015, **34**, 1601-1603.
21. Y. Tomita, S. Teruya, O. Koga and Y. Hori, *J. Electrochem. Soc.*, 2000, **147**, 4164-4167.
22. J. E. Heimann, W. H. Bernskoetter, N. Hazari and J. M. Mayer, *Chem Sci*, 2018, **9**, 6629-6638.
23. Z. Wang, Y. Zhang, M. Kurmoo, T. Liu, S. Vilminot, B. Zhao and S. Gao, *Aust. J. Chem.*, 2006, **59**, 617-628.
24. Y. Peng, Y. Li, Y. Ban, H. Jin, W. Jiao, X. Liu and W. Yang, *Science*, 2014, **346**, 1356-1359.
25. C. V. Picasso, D. A. Safin, I. Dovgaliuk, F. Devred, D. Debecker, H.-W. Li, J. Proost and Y. Filinchuk, *Int. J. Hydrog. Energy*, 2016, **41**, 14377-14386.
26. N. B. McKeown and P. M. Budd, *Chem. Soc. Rev.*, 2006, **35**, 675-683.
27. T. Ben, H. Ren, S. Ma, D. Cao, J. Lan, X. Jing, W. Wang, J. Xu, F. Deng, J. M. Simmons, S. Qiu and G. Zhu, *Angew. Chem. Int. Ed.*, 2009, **121**, 9621-9624.
28. C. Zhou, L. Longley, A. Krajnc, G. J. Smales, A. Qiao, I. Erucar, C. M. Doherty, A. W. Thornton, A. J. Hill, C. W. Ashling, O. T. Qazvini, S. J. Lee, P. A. Chater, N. J. Terrill, A. J. Smith, Y. Yue, G. Mali, D. A. Keen, S. G. Telfer and T. D. Bennett, *Nat. Commun.*, 2018, **9**, 5042.
29. A. Giannis and K. Sandhoff, *Angew. Chem. Int. Ed.*, 1989, **28**, 218-220.
30. H. Furukawa, N. Ko, Y. B. Go, N. Aratani, S. B. Choi, E. Choi, A. Ö. Yazaydin, R. Q. Snurr, M. O'Keeffe, J. Kim and O. M. Yaghi, *Science*, 2010, **329**, 424-428.
31. M. Kawano, T. Haneda, D. Hashizume, F. Izumi and M. Fujita, *Angew. Chem. Int. Ed.*, 2008, **47**, 1269-1271.